Advances in Nano Research, *Vol. 19, No. 4 (2025) 367-382*
https://doi.org/10.12989/anr.2025.19.4.367

Static behavior of power-law coated porous functionally graded metal foam shells

Ahmed Amine Daikh*[1,2], Mohamed A Eltaher[3], Rania Gamal[4], Loubna Nadji[1] and Norhan A. Mohamed[5]

[1]*Artificial Intelligence Laboratory for Mechanical and Civil Structures, and Soil, University Centre of Naama, P.O. Box 66, Naama 45000, Algeria*
[2]*Laboratoire d'Etude des Structures et de Mécanique des Matériaux, Département de Génie Civil, Faculté des Sciences et de la Technologie, Université Mustapha Stambouli B.P. 305, R.P.29000 Mascara, Algérie*
[3]*Mechanical Engineering Department, Faculty of Engineering, King Abdulaziz University, P.O. Box 80204, Jeddah 21589, Saudi Arabia*
[4]*Faculty of Engineering Technology Elsewedy University of Technology-Polytechnic Egypt Cairo 7060010, Egypt*
[5]*Engineering Mathematics Department, Faculty of Engineering, Zagazig University, Zagazig, 44519, Egypt*

(*Received March 23, 2025, Revised August 22, 2025, Accepted September 23, 2025*)

Abstract. The advancement of theoretical research faces numerous challenges, particularly when it comes to modeling structures, in contrast to the experimental investigation of the mechanical behavior of complex systems. Metal foams are advanced composite materials with high porosity, low weight, and excellent thermal conductivity, making them essential for applications in thermal management, filtration, catalysis, and energy storage. The study addresses the challenges in theoretical research related to modeling complex structures, presenting a more accurate approach by incorporating nonclassical mechanics. It introduces a novel method for modeling tri-directionally coated porous structures with varying microstructures, accounting for intrinsic characteristic lengths and spatial variations in material properties. The study focuses on the static behavior of multidirectionally functionally graded porous metal foam shells, utilizing modified higher-order shear deformation theory and the principle of virtual work. To tackle various boundary conditions, the investigation employs the Galerkin method, providing a comprehensive and refined analysis of the system's behavior. Two types of porous shells, categorized as Softcore (SC) and Hardcore (HC), are analyzed, with five distribution patterns: tri-directional (Type-A), two bidirectional (Type-B and Type-C), transverse unidirectional (Type-D), and axial unidirectional (Type-E).

Keywords: bending response; gGalerkin procedure; Modified higher-order shear deformation theory; 3D material distribution

1. Introduction

Characterized by their curved, thin-walled design, shell structures play a vital role in aerospace, automotive, marine engineering, turbomachinery, and pressure vessel applications (Punera and Kant 2019). In civil and mechanical engineering, they are commonly used in slabs, vaults, roofs, domes, chimneys, cooling towers, pipes, tanks, and pressure vessels (Radwańska *et al.* 2017). Despite significant research on their static behavior, the topic remains an active and evolving field of study.

Recent studies have considered structures composed of various material constituents. Medjdoubi *et al.* (2023) developed a novel analytical model to investigate how porosity influences the shear correction factors (SCFs) in functionally graded porous beams (FGPBs). In this study, the porosity distribution across the beam thickness is characterized using uneven and logarithmic-uneven functions. Garg *et al.* (2022) attempted to evaluate the stiffness matrix of functionally graded (FG) nannoplates using a Gaussian process regression (GPR)-based surrogate model within the framework of layerwise theory. Abouelregal *et al.* (2021) examined the thermal and mechanical vibration behavior of functionally graded microbeams by formulating the governing equations based on the classical Euler–Bernoulli beam model and the generalized dual-phase lag model of thermoelasticity, instead of the conventional steady-state Fourier heat conduction. Garg *et al.* (2022) investigated the bending behavior of sandwich functionally graded (FGM) beams under thermal loading using shear deformation theory, incorporating temperature-dependent material properties in the analysis. Melaibari *et al.* (2022a, b) investigated the vibration characteristics of composite shells reinforced with randomly oriented single-walled carbon nanotubes and FG fibers. Ladmek *et al.* (2023) developed an analytical method based on higher-order shear deformation theory to study the free vibration behavior of functionally graded carbon nanotube-reinforced composite beams, where material gradation and properties are represented using cosine functions. Tornabene *et al.* (2023) developed a Layer-Wise model for the static analysis of doubly curved shells under general boundary conditions. Yıldız and Esen (2023a) modeled and studied the thermomechanical buckling behavior of sandwich nanoplates with foam core layers using nonlocal strain gradient elasticity theory and a unique higher order deformation theory. In a separate study, Yıldız and Esen (2023b) simulate the thermomechanical vibrational behavior of sandwich nanoplates comprising a foam or solid

*Corresponding author, Ph.D.,
E-mail: daikhresearch@gmail.com

ISSN: 2287-237X (Print), 2287-2388 (Online)

core layer and intelligent surface layers, incorporating the effects of nanoscale dimensions, nonlocal strain gradient theory, and sinusoidal higher-order plate theory. Abdelhaffez *et al*. (2023) formulated a mathematical model for the buckling of coated FG shells resting on an orthotropic elastic medium. Garg *et al*. (2022) conducted bending and free vibration analyses of multilayered functionally graded graphene platelet (GPL) and fiber-reinforced hybrid composite beams using shear deformation theory based on a parabolic function. Shariati *et al*. (2020) conducted numerical and analytical studies on the size-dependent vibrations and stability of moving viscoelastic axially functionally graded (AFG) nanobeams, with the goal of improving the stability of translating nanosystems, and also provided a parametric analysis to examine the effects of factors such as axial material gradation, viscosity coefficient, and nonlocal parameter on the system's stability boundaries. Garg *et al*. (2023) performed a free vibration analysis of power-law and sigmoidal sandwich plates composed of FGMs using finite element-based higher-order zigzag theory. Esen *et al*. (2024) examined the thermos-mechanical buckling characteristics of sandwich plates composed of functionally graded layers, isotropic layers, and foam core layers, utilizing sinusoidal higher-order shear theory. The energy equation of the sandwich plate integrates the displacement and strain of each layer into the equations of motion, accounting for the nonlinearity of temperature increase. Chau-Dinh (2023) proposed an enhanced three-node triangular flat shell element with a bubble function and cell-based strain smoothing for static analysis. Sedighi *et al*. (2020) and Sedighi and Malikan (2020) studied instability analysis of fluid-conveying C-BN hybrid-nanotube in a magneto-thermal environment by using stress-driven nonlocal elasticity. Garg *et al*. (2023) conducted a bending analysis of sandwich functionally graded (FG) beams under thermal conditions using Navier's solution-based parabolic shear deformation theory, presenting a comparative study of exponential and sigmoidal sandwich FGM beams. Hieu *et al*. (2021) provided a comprehensive theoretical framework for the nonlinear bending, vibration and buckling of functionally graded (FG) nanobeams resting on an elastic foundation through nonlocal strain gradient theory. Eroğlu *et al*. (2025a) examined the thermo-mechanical free vibration and buckling properties of doubly-curved sandwich shell structures, which comprise a core of functionally graded graphene-reinforced foam and metal or ceramic facing layers. They utilized Hamilton's principle and a Navier-type solution method to establish governing equations and boundary conditions for simply supported setups. The same authors (Eroğlu *et al*. 2025b) investigated the phenomenon of three-dimensional wave propagation in doubly-curved sandwich shell constructions, which have a core made of functionally graded foam, with upper and lower layers of metal and ceramic. The research highlights the thermo-mechanical properties intrinsic to these materials. Jena *et al*. (2022) investigated the effect of geometrical uncertainties on the free vibration of Euler–Bernoulli FG beams resting on Winkler-Pasternak elastic foundation. Ghandourah *et al*. (2023) studied the dynamic behavior of porous coated FG nanoshells resting on a viscoelastic medium. Son *et al*. (2024) studied the role of temperature and nonlocality on the low- and high-frequency behaviors of FG sandwich nanoplates resting on Winkler–Pasternak foundations. Tharwan *et al*. (2023) studied the static behavior of agglomerated coated FG carbon nanotube-reinforced composite nanoshells supported by a complex elastic foundation. A highly efficient nonlocal finite element model is introduced to analyze the bending and buckling behavior of functionally graded (FG) nanobeams, incorporating a newly developed two-node beam element with eight degrees of freedom based on the advanced higher-order shear deformation theory by Belarbi *et al*. (2021). Do *et al*. (2023) provided closed-form solutions for the elastic–plastic buckling of shell structures under external pressure. Khaniki and Ghayesh (2023) applied Donnell's nonlinear shell theory and the Mooney-Rivlin strain energy density model to hyperelastic shell structures. Garg *et al*. (2021) offer an extensive review of sandwich FGM structures, focusing on their use as structural elements and examining various methods and theories for analyzing them under different loading conditions. Daikh *et al*. (2023) evaluated buckling loads and bending deflection in coated FG graphene-reinforced composite plates and shells using the Galerkin technique. Hadji *et al*. (2024) proposed a displacement-based high-order shear deformation theory for the static response of functionally graded plates, which is variationally consistent and closely resembles classical plate theory in many respects, eliminating the need for the shear correction factor. Rezov (2024) presents a theoretical study on delamination in U-shaped load-carrying structural members, which are multilayered functionally graded systems exhibiting non-linear viscoelastic behavior. The delamination occurs in the right-hand vertical section of the structure, which is clamped at the lower end of the left-hand vertical part and supported by a rotational spring with non-linear elastic behavior. Dang *et al*. (2021) developed a model for a functionally graded (FG) nanotube conveying fluid, embedded in an elastic medium, based on the nonlocal strain gradient theory (NSGT) combined with Euler-Bernoulli beam theory (EBT), aiming to analyze the nonlinear vibrations and stability of fluid-conveying nanotubes.

Porous materials are gaining widespread attention due to their favorable properties, such as low specific weight, excellent energy absorption, low thermal and electrical conductivity, high specific strength, and improved recyclability and machinability (Keleshteri and Jelovica, 2022). In addition, coated functionally graded materials are widely used in various industrial applications, including turbine blades, cutting tools, and aircraft engines, due to their superior mechanical properties and ability to withstand extreme conditions. Studying the static response of fully coated functionally graded nanoshells is essential for understanding their behavior under different loading conditions, which is crucial for optimizing their design and ensuring their performance and durability in these high-performance applications.

Despite extensive research, the static analysis of three-dimensional porous metal foam shells has not been thoroughly explored. This study aims to address this gap by presenting a comprehensive analysis of such structures. The

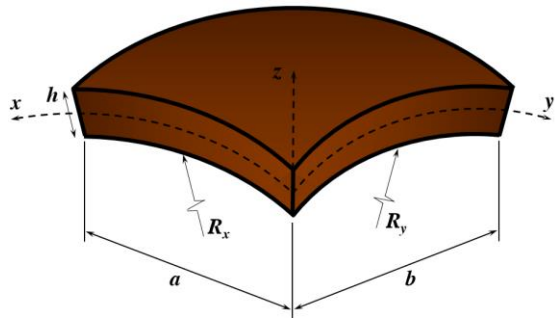

Fig. 1 FG spherical shell geometry

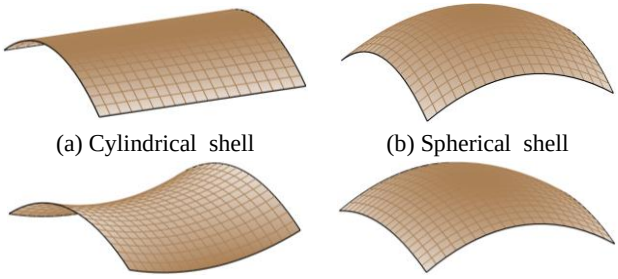

(a) Cylindrical shell (b) Spherical shell

(c) Hyperbolic-Paraboloid shell (d) Elliptical-Paraboloid shell

Fig. 2 Forms of various shells

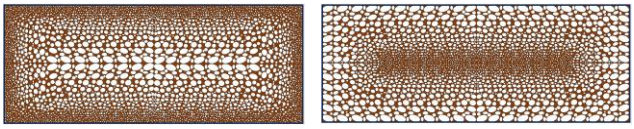

(a) 2D SC surface porosity distribution (b) 2D HC surface porosity distribution

Fig. 3 Porosity distribution through plate surface

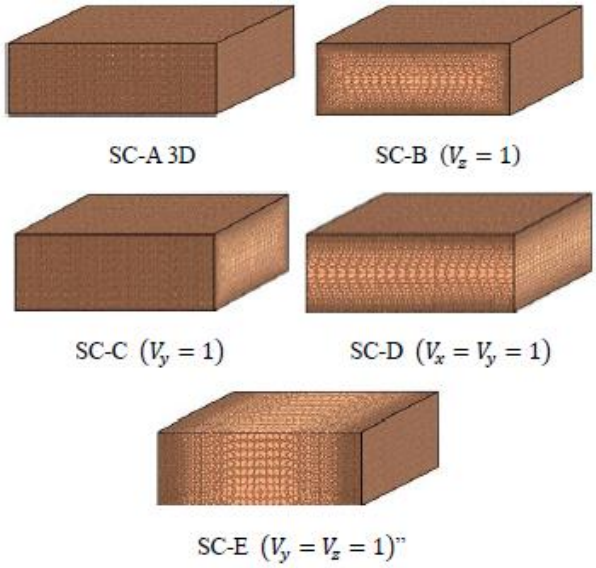

Fig. 4 Various schemes of SC porous shell ($R_x = R_y = \infty$)

proposed approach utilizes nonclassical mechanics to model innovative tri-directionally coated porous structures with varying microstructures, incorporating intrinsic characteristic lengths and spatial variations in material properties for improved accuracy. The proposed model is limited to the static behavior of shells, specifically uniform cross-sectional nanoshells with fixed and hinged boundary conditions.

2. Geometrical and material distribution

The composite shell under investigation is defined by its dimensions: length (a), width (b), and thickness (h) (Fig. 1). It encompasses various geometrical configurations, including cylindrical, spherical, elliptical–paraboloid, and hyperbolic–paraboloid shells (Fig. 2). The shell's midplane features two principal curvature radii, R_x and R_y, corresponding to the x- and y-directions, respectively.

This structure is composed of porous metal foam, with an analysis of two distinct pore distribution types: hardcore and softcore (Fig. 3). Additionally, five unique pore distribution patterns are considered:

– FG-A – A tridirectional material distribution pattern

– Type-B – A bidirectional material distribution pattern

– Type-C – A second bidirectional material distribution pattern

– Type-D – A unidirectional transverse material distribution pattern

– Type-E – A unidirectional axial material distribution pattern

(Figs. 4 illustrates these patterns).

The effective elastic modulus (E) and shear modulus (G) for both pore distribution types are expressed as follows:

$$\begin{aligned} E(x,y,z) &= E0_{max} \\ G(x,y,z) &= G0_{max} \end{aligned} \tag{1}$$

Here, E_{max} and G_{max} are the maximum values of Young's modulus and shear modulus, respectively. The porosity coefficient is presented by e_0, where:

$$e_0 = 1 - \frac{E_{min}}{E_{max}=1-\frac{G_{min}}{G_{max}}} \tag{2}$$

where E_{min} and G_{min} denote the minimum values of Young's modulus and shear modulus, respectively. The parameter e_0 varies within the range $0<e_0<1$.

The volume fraction $V(x,y,z)$ is defined by three independent formulas, each corresponding to a specific spatial direction:

$$\begin{aligned} V(x,y,z) &= V(x)V(y)V(z) \quad \text{for SC shells} \\ V(x,y,z) &= 1 - V(x)V(y)V(z) \quad \text{for HC shells} \end{aligned} \tag{3}$$

where

$$\begin{aligned} V(x) &= \left(1 - \frac{|\,2x-a\,|}{a}\right)^p \\ V(y) &= \left(1 - \frac{|\,2y-b\,|}{b}\right)^k \\ V(z) &= \left(1 - 2\frac{|\,z\,|}{h}\right)^e \end{aligned} \tag{4}$$

3. Displacement field

In specific cases, where the shell has a uniform thickness and the boundary conditions at opposite ends are identical (e.g., SSSS, CCCC, CCSS), the formulations for

the shells are developed using a shear deformation theory based on an inverse trigonometric function. The displacement field is expressed as follows (Ghandourah *et al.* 2023):

$$\begin{aligned} u(x,y,z) &= \left(1+\frac{z}{R_x}\right)u_0 - z\frac{\partial w_0}{\partial x} - f(z)\frac{\partial \psi}{\partial x} \\ v(x,y,z) &= \left(1+\frac{z}{R_y}\right)v_0 - z\frac{\partial w_0}{\partial y} - f(z)\frac{\partial \psi}{\partial y} \\ w(x,y,z) &= w_0 \end{aligned} \tag{5}$$

The midplane displacements of the shell are denoted as u_0, v_0, and w_0, while the transverse normal rotations at $z = 0$ are represented by ψ. The shape function $f(z)$ is defined as:

$$f(z) = h\,sinh\left(\frac{z}{h}\right) - \frac{3z^3}{2h^2} \tag{6}$$

The strains can be obtained by differentiating the displacement equation provided earlier:

$$\begin{aligned} &\begin{Bmatrix}\varepsilon_{xx}\\ \varepsilon_{yy}\\ \gamma_{xy}\end{Bmatrix} = \begin{Bmatrix}\varepsilon^0_{xx}\\ \varepsilon^0_{yy}\\ \gamma^0_{xy}\end{Bmatrix} + z\begin{Bmatrix}\varepsilon^1_{xx}\\ \varepsilon^1_{yy}\\ \gamma^1_{xy}\end{Bmatrix} + f(z)\begin{Bmatrix}\varepsilon^2_{xx}\\ \varepsilon^2_{yy}\\ \gamma^2_{xy}\end{Bmatrix}, \\ &\varepsilon_{zz} = 0, \quad \begin{Bmatrix}\gamma_{yz}\\ \gamma_{xz}\end{Bmatrix} = \frac{df(z)}{dz}\begin{Bmatrix}\gamma^0_{yz}\\ \gamma^0_{xz}\end{Bmatrix} \end{aligned} \tag{7}$$

where

$$\begin{aligned} &\begin{Bmatrix}\varepsilon^0_{xx}\\ \varepsilon^0_{yy}\\ \gamma^0_{xy}\end{Bmatrix} = \begin{Bmatrix} u_{0,x} + \dfrac{w_0}{R_x} \\ v_{0,y} + \dfrac{w_0}{R_y} \\ v_{0,x} + u_{0,y}\end{Bmatrix}, \quad \begin{Bmatrix}\varepsilon^1_{xx}\\ \varepsilon^1_{yy}\\ \gamma^1_{xy}\end{Bmatrix} = -\begin{Bmatrix} w_{0,xx} \\ w_{0,yy} \\ 2w_{0,xy}\end{Bmatrix}, \\ &\begin{Bmatrix}\varepsilon^2_{xx}\\ \varepsilon^2_{yy}\\ \gamma^2_{xy}\end{Bmatrix} = \begin{Bmatrix} \psi_{,xx} \\ \psi_{,yy} \\ -2\psi_{,xy}\end{Bmatrix}, \quad \begin{Bmatrix}\gamma^0_{yz}\\ \gamma^0_{xz}\end{Bmatrix} = \begin{Bmatrix}\psi_{,y}\\ \psi_{,x}\end{Bmatrix} \end{aligned} \tag{8}$$

The stress-strain relationships are given by:

$$\begin{Bmatrix}\sigma_{xx}\\ \sigma_{yy}\\ \tau_{yz}\\ \tau_{xz}\\ \tau_{xy}\end{Bmatrix} = \begin{bmatrix} Q_{11} & Q_{12} & 0 & 0 & 0 \\ Q_{12} & Q_{22} & 0 & 0 & 0 \\ 0 & 0 & 0 & Q_{44} & 0 \\ 0 & 0 & Q_{55} & 0 & 0 \\ 0 & 0 & 0 & 0 & Q_{66}\end{bmatrix}\begin{Bmatrix}\varepsilon_{xx}\\ \varepsilon_{yy}\\ \gamma_{yz}\\ \gamma_{xz}\\ \gamma_{xy}\end{Bmatrix} \tag{9}$$

where

$$\begin{aligned} &Q_{11} = \frac{E}{1-\nu^2}, \quad Q_{22} = Q_{11}, \quad Q_{12} = \frac{\nu E}{1-\nu^2}, \\ &Q_{44} = Q_{55} = Q_{66} = \frac{E}{2(1+\nu)} \end{aligned} \tag{10}$$

Integrating Eq. (32) yields the expressions for the stress resultants, moments, and additional moment resultants as follows:

$$\begin{Bmatrix}\{N\}\\ \{M\}\\ \{P\}\end{Bmatrix} = \begin{bmatrix}[A] & [B] & [C] \\ [B] & [D] & [F] \\ [C] & [F] & [H]\end{bmatrix}\begin{Bmatrix}\{\varepsilon^0\}\\ \{\varepsilon^1\}\\ \{\varepsilon^2\}\end{Bmatrix} \tag{11}$$

$$\begin{Bmatrix}R_{yz}\\ R_{xz}\end{Bmatrix} = \begin{bmatrix}J_{44} & J_{45}\\ J_{45} & J_{55}\end{bmatrix}\begin{Bmatrix}\gamma^0_{yz}\\ \gamma^0_{xz}\end{Bmatrix} \tag{12}$$

where

$$\{N\} = \{N_{xx} \quad N_{yy} \quad N_{xy}\}^T, \tag{13}$$

$$\begin{aligned} &\{M\} = \{M_{xx} \quad M_{yy} \quad M_{xy}\}^T, \\ &\{P\} = \{P_{xx} \quad P_{yy} \quad P_{xy}\}^T \\ &\{\varepsilon^0\} = \{\varepsilon^0_{xx} \quad \varepsilon^0_{yy} \quad \gamma^0_{xy}\}^T, \\ &\{\varepsilon^1\} = \{\varepsilon^1_{xx} \quad \varepsilon^1_{yy} \quad \gamma^1_{xy}\}^T, \\ &\{\varepsilon^2\} = \{\varepsilon^2_{xx} \quad \varepsilon^2_{yy} \quad \gamma^2_{xy}\}^T\{\varepsilon^0\} \end{aligned}$$

and

$$\begin{aligned} &A_{ij}, B_{ij}, D_{ij}, C_{ij}, F_{ij}, H_{ij} = \\ &\int_{-h/2}^{h/2} Q_{ij}\{1, z, z^2, f(z), zf(z), [f(z)]^2\}dz, \quad (i,j = 1,2,6) \\ &J_{ii} = \int_{-h/2}^{h/2} Q_{ii}\left[\frac{df(z)}{dz}\right]^2 dz, \quad (i = 4,5) \end{aligned} \tag{14}$$

4. Equilibrium equations

To derive the equilibrium equations, the potential energy principle is employed, given by;

$$\int_V \sigma_{ij}\,\delta\varepsilon_{ij}\,dV - \int_A q\delta w\,dA = 0 \tag{15}$$

The symbol q denotes the distributed transverse load. By integrating the strains and stresses, the potential energy principle is formulated as:

$$\delta U = \int \begin{bmatrix} N_{xx}\dfrac{\partial u}{\partial x} - M_{xx}\dfrac{\partial^2 w}{\partial x^2} - S_{xx}\dfrac{\partial^2 \psi}{\partial x^2} + N_{yy}\dfrac{\partial v}{\partial y} \\ -M_{yy}\dfrac{\partial^2 w}{\partial y^2} - S_{yy}\dfrac{\partial^2 \psi}{\partial y^2} + N_{xy}\left(\dfrac{\partial u}{\partial y} + \dfrac{\partial v}{\partial x}\right) \\ -2M_{xy}\dfrac{\partial^2 w}{\partial x \partial y} - 2S_{xy}\dfrac{\partial^2 \psi}{\partial x \partial y} - q\delta w \end{bmatrix} \tag{16}$$

Substituting Eqs. (8, 9, 11) into Eq (16) yields the equilibrium equations for the shell, as follows

$$\begin{aligned} &(A_{12}+A_{66})\frac{\partial^2 u_0}{\partial x \partial y} + A_{22}\frac{\partial^2 v_0}{\partial y^2} + A_{66}\frac{\partial^2 v_0}{\partial x^2} \\ &-(B_{12}+2B_{66})\frac{\partial^3 w_0}{\partial x^2 \partial y} - B_{22}\frac{\partial^3 w_0}{\partial y^3} \\ &+\left(\frac{A_{12}}{R_x}+\frac{A_{22}}{R_y}\right)\frac{\partial w_0}{\partial y} - (C_{12}+2C_{66})\frac{\partial^3 \psi}{\partial x^2 \partial y} \\ &-C_{22}\frac{\partial^3 \psi}{\partial y^3} = 0 \end{aligned} \tag{17}$$

$$\begin{aligned} &(A_{12}+A_{66})\frac{\partial^2 u_0}{\partial x \partial y} + A_{22}\frac{\partial^2 v_0}{\partial y^2} + A_{66}\frac{\partial^2 v_0}{\partial x^2} \\ &-(B_{12}+2B_{66})\frac{\partial^3 w_0}{\partial x^2 \partial y} - B_{22}\frac{\partial^3 w_0}{\partial y^3} \\ &+\left(\frac{A_{12}}{R_x}+\frac{A_{22}}{R_y}\right)\frac{\partial w_0}{\partial y} - (C_{12}+2C_{66})\frac{\partial^3 \psi}{\partial x^2 \partial y} \\ &-C_{22}\frac{\partial^3 \psi}{\partial y^3} = 0 \end{aligned} \tag{18}$$

$$\begin{aligned} &B_{11}\frac{\partial^3 u_0}{\partial x^3} + (B_{12}+2B_{66})\frac{\partial^3 u_0}{\partial x \partial y^2} - \left(\frac{A_{11}}{R_x}+\frac{A_{12}}{R_y}\right)\frac{\partial u_0}{\partial x} \\ &+(B_{12}+2B_{66})\frac{\partial^3 v_0}{\partial x^2 \partial y} + B_{22}\frac{\partial^3 v_0}{\partial y^3} \end{aligned} \tag{19}$$

$$
\begin{aligned}
&-\left(\frac{A_{12}}{R_x}+\frac{A_{22}}{R_y}\right)\frac{\partial v_0}{\partial y}+\left(\frac{2B_{11}}{R_x}+\frac{2B_{12}}{R_y}\right)\frac{\partial^2 w_0}{\partial x^2}\\
&-D_{11}\frac{\partial^4 w_0}{\partial x^4}-(2D_{12}+4D_{66})\frac{\partial^4 w_0}{\partial x^2\partial y^2}-D_{22}\frac{\partial^4 w_0}{\partial y^4}\\
&+\left(\frac{2B_{12}}{R_x}+\frac{2B_{22}}{R_y}\right)\frac{\partial^2 w_0}{\partial y^2}-\left(\frac{A_{11}}{R_x^2}+2\frac{A_{12}}{R_xR_y}+\frac{A_{22}}{R_y^2}\right)w_0\\
&-E_{11}\frac{\partial^4 \psi}{\partial x^4}-2(E_{12}+2E_{66})\frac{\partial^4 \psi}{\partial x^2\partial y^2}-E_{22}\frac{\partial^4 \psi}{\partial y^4}\\
&+\left(\frac{C_{11}}{R_x}+\frac{C_{12}}{R_y}\right)\frac{\partial^2 \psi}{\partial x^2}+\left(\frac{C_{12}}{R_x}+\frac{C_{22}}{R_y}\right)\frac{\partial^2 \psi}{\partial y^2}+q=0
\end{aligned}
$$

$$
\begin{aligned}
&C_{11}\frac{\partial^3 u}{\partial x^3}+(C_{12}+2C_{66})\frac{\partial^3 u}{\partial x\partial y^2}\\
&+(C_{12}+2C_{66})\frac{\partial^3 v}{\partial x^2\partial y}+C_{22}\frac{\partial^3 v}{\partial y^3}-E_{11}\frac{\partial^4 w_0}{\partial x^4}\\
&-2(E_{12}+2E_{66})\frac{\partial^4 w_0}{\partial x^2\partial y^2}-E_{22}\frac{\partial^4 w_0}{\partial y^4}-F_{11}\frac{\partial^4 \psi}{\partial x^4}\\
&-2(F_{12}+2F_{66})\frac{\partial^4 \psi}{\partial x^2\partial y^2}-F_{22}\frac{\partial^4 \psi}{\partial y^4}+J_{44}\frac{\partial^2 \psi}{\partial y^2}\\
&+J_{55}\frac{\partial^2 \psi}{\partial x^2}+\left(\frac{C_{11}}{R_x}+\frac{C_{12}}{R_y}\right)\frac{\partial^2 w}{\partial x^2}+\left(\frac{C_{12}}{R_x}+\frac{C_{22}}{R_y}\right)\frac{\partial^2 w}{\partial y^2}=0
\end{aligned}
\tag{20}
$$

5. Analytical solution

A key objective of this research is to broaden the use of analytical solutions for assessing the response of various structural forms, including shell structures, under different boundary conditions. To achieve this, the Galerkin method is employed to obtain accurate solutions. The generalized displacements are expressed as follows:

$$
\begin{aligned}
u_0&=\sum_{m=1}^{\infty}\sum_{n=1}^{\infty} U_{mn}\cdot\frac{\partial X_m(x)}{\partial x}Y_n(y)\\
v_0&=\sum_{m=1}^{\infty}\sum_{n=1}^{\infty} V_{mn}\cdot X_m(x)\frac{\partial Y_n(y)}{\partial y}\\
\{w_0,\psi\}&=\sum_{m=1}^{\infty}\sum_{n=1}^{\infty}\{W_{mn},\Psi_{mn}\}X_m(x)Y_n(y)
\end{aligned}
\tag{21}
$$

U_{mn}, V_{mn}, W_{mn}, and Ψ_{mn} are arbitrary parameters. Table 2 contains the functions $X_m(x)$ and $Y_n(y)$ that satisfy the above boundary conditions.

The parameters U_{mn}, V_{mn}, W_{mn}, X_{mn} and Z_{mn} are arbitrary. Table 1 presents the functions $X_m(x)$ and $Y_n(y)$ that meet the aforementioned boundary conditions.

The externally applied transverse sinusoidal load can be defined as follows:

$$
q=-q_0\int_0^a\int_0^b \sin^2(\alpha x)\sin^2(\beta y)\,dx\,dy \tag{22}
$$

where q_0 is the maximum load intensity. By substituting Eq. (21) in Eqs. (17-20), one obtains

$$
[K]_{4\times4}\begin{Bmatrix}U_{mn}\\V_{mn}\\W_{mn}\\\Psi_{mn}\end{Bmatrix}=\begin{Bmatrix}0\\0\\q\\0\end{Bmatrix} \tag{23}
$$

where [K] and [M] are the rigidity matrix and mass matrix, respectively. The elements K_{ij} and M_{ij} of the matrix [K] and [M] are given in Appendix A.

Table 1 The admissible functions $X_m(x)$ and $Y_n(y)$

BCs.	The functions X_m and Y_n	
	$X_m(x)$	$Y_n(y)$
SSSS	$\sin(\alpha x)$	$\sin(\beta y)$
CCCC	$\sin^2(\alpha x)$	$\sin^2(\beta y)$
CCSS	$\sin^2(\alpha x)$	$\sin(\beta y)$

6. Results and discussions

A detailed numerical analysis is conducted to investigate the static behavior of multidirectional porous metal foam shells. The study focuses on the effects of key parameters, including porosity distribution, porosity coefficient, shell geometry, and different boundary conditions. The results are systematically presented in tables and graphs. The analysed shell are assumed to be constructed from open-cell steel foam, with the following material properties: a maximum Young's modulus $E_{max}=200$ GPa and a Poisson's ratio $=1/3$. The normalized stresses and deflection are calculated using:

$$
\overline{w}=\frac{10E3_{max}}{a^2q_0\left(\frac{a}{2},\frac{b}{2},z\right)} \tag{24}
$$

$$
\overline{\sigma}_{xx}=\frac{ah}{q_0}\sigma_{xx}\left(\frac{a}{2},\frac{b}{2},\frac{h}{2}\right) \tag{25}
$$

$$
\overline{\tau}_{xx}=\frac{ah}{q_0}\tau_{xz}\left(0,\frac{b}{2},0\right) \tag{26}
$$

The numerical investigation evaluates the influence of the porosity coefficient, power-law indices, and distribution patterns on the central deflection as shown in Table 2 and Table 3, axial stress in Table 4, and shear stress in Table 5.

The influence of power-law parameters on the dimensionless central deflection for various porous spherical shells is illustrated in Fig. 5. When *p*=*k*=*e*=0, the porosity distribution is uniform, which explains the consistent results observed across different porosity distribution patterns. For spherical shells with a softcore, an increase in the power-law parameters *p*, *k* and *e* leads to a reduction in dimensionless central deflections. In contrast, for shells with a hardcore, this trend does not hold. Among SC shells, the functionally graded pattern FG-E exhibits the highest rigidity, while for HC shells, the HC-A pattern is the most rigid.

Fig. 6 illustrates the distribution of axial stresses across varying values of the porosity coefficient and power-law indices. For SC-A shells, a linear variation in axial stress is observed when *p*=0, which is attributed to the uniform distribution of porosities. Notably, the maximum stresses consistently occur at the top section of the shell, regardless of the SC distribution patterns or inhomogeneity parameters. This highlights the critical role of porosity distribution and power-law indices in influencing stress localization and overall structural behavior.

Table 2 Effect of porosity coefficient on dimensionless central deflection $\bar{w}$ of various patterns of porous shells (p=k=e=0.5SSSS, a=b=10h)

Shell(*)	e_0	SC-A	SC-B	SC-C	SC-D	SC-E	HC-A	HC-B	HC-C	HC-D	HC-E
plate	0.2	3.02752	3.18248	3.09596	3.20484	3.34569	3.44309	3.26204	3.35918	3.24084	3.10671
	0.4	3.16767	3.52653	3.32201	3.58568	3.95399	4.23826	3.72805	3.9935	3.67568	3.34569
	0.6	3.32201	3.95399	3.58568	4.07855	4.83266	5.51352	4.34939	4.92654	4.24917	3.62449
	0.8	3.49300	4.49937	3.89848	4.75797	6.21342	7.89586	5.21927	6.43688	5.04096	3.95399
Cylindrical	0.2	2.94368	3.0928	3.01102	3.11823	3.25141	3.34416	3.17012	3.26178	3.14569	3.01917
	0.4	3.08163	3.42716	3.23369	3.49381	3.84257	4.11300	3.6230	3.87319	3.5622	3.25141
	0.6	3.23369	3.84257	3.49381	3.98113	4.69648	5.34330	4.22683	4.76988	4.10948	3.52236
	0.8	3.40232	4.37258	3.80293	4.65461	6.03833	7.63248	5.0722	6.21464	4.86126	3.84257
Spherical	0.2	2.71789	2.85173	2.78206	2.88438	2.99797	3.07875	2.92302	3.00077	2.89105	2.78383
	0.4	2.84942	3.16002	2.99481	3.24443	3.54306	3.77805	3.3406	3.55217	3.26025	2.99797
	0.6	2.99481	3.54306	3.24443	3.71492	4.3304	4.89037	3.89736	4.35447	3.74056	3.2478
	0.8	3.15651	4.03175	3.54248	4.36986	5.56766	6.93817	4.67683	5.63136	4.39159	3.54306
Hyperbolic-paraboloid	0.2	2.80556	2.94526	2.871	2.97529	3.0963	3.18163	3.01889	3.10190	2.98965	2.87513
	0.4	2.93967	3.26367	3.08774	3.3416	3.65926	3.90770	3.45016	3.67631	3.37686	3.0963
	0.6	3.08774	3.65926	3.3416	3.81896	4.47243	5.06530	4.02519	4.51465	3.88256	3.35432
	0.8	3.25224	4.16399	3.64416	4.48155	5.75027	7.20520	4.83022	5.85525	4.57153	3.65926
Elliptical-paraboloid	0.2	3.02752	3.18248	3.09596	3.20484	3.34569	3.44309	3.26204	3.35918	3.24084	3.10671
	0.4	3.16767	3.52653	3.32201	3.58568	3.95399	4.23826	3.72805	3.99350	3.67568	3.34569
	0.6	3.32201	3.95399	3.58568	4.07855	4.83266	5.51352	4.34939	4.92654	4.24917	3.62449
	0.8	3.49300	4.49937	3.89848	4.75797	6.21342	7.89586	5.21927	6.43688	5.04096	3.95399

(*) Plate: $R_x = R_y = \infty$, Cylindrical: $R_x = 5, R_y = \infty$, Spherical: $R_x = R_y = 5$, Hyperbolic-paraboloid: $R_x = 5, R_y = 7.5$, Elliptical-paraboloid: $R_x = -R_y = 5$

Table 3 Effect of power-law coefficient on dimensionless central deflection of various patterns of porous shells (e_0=0.5SSSS, a=b=10h)

Shell(*)	p=k=e	SC-A	SC-B	SC-C	SC-D	SC-E	HC-A	HC-B	HC-C	HC-D	HC-E
plate	0.00	5.79919	5.79919	5.79919	5.79919	5.79919	2.89960	2.89960	2.89960	2.89960	2.89960
	0.25	3.68993	4.26411	3.96078	4.36216	4.83266	4.06424	3.53609	3.78174	3.47951	3.22177
	0.50	3.24293	3.72805	3.44853	3.81484	4.34939	4.79219	4.01482	4.41081	3.94123	3.47951
	0.75	3.07780	3.46537	3.22799	3.53509	4.05943	5.20292	4.3717	4.83304	4.30079	3.69039
Cylindrical	1.00	3.00217	3.31382	3.11353	3.36962	3.86613	5.43234	4.63935	5.11247	4.57865	3.86613
	0.00	5.63578	5.63578	5.63578	5.63578	5.63578	2.81789	2.81789	2.81789	2.81789	2.81789
	0.25	3.59134	4.14395	3.85690	4.2509	4.69648	3.94309	3.43645	3.668	3.37385	3.13099
	0.50	3.15575	3.623	3.35845	3.72022	4.22683	4.64783	3.90169	4.27464	3.8159	3.38147
Spherical	0.75	2.99424	3.36772	3.1431	3.44802	3.94504	5.04712	4.24851	4.68293	4.16021	3.5864
	1.00	2.91999	3.22044	3.03096	3.28656	3.75718	5.27127	4.50862	4.95417	4.42664	3.75718
	0.00	5.19648	5.19648	5.19648	5.19648	5.19648	2.59824	2.59824	2.59824	2.59824	2.59824
	0.25	3.32483	3.82094	3.57557	3.94876	4.3304	3.61941	3.16859	3.36442	3.09218	2.88693
Hyperbolic-paraboloid	0.50	2.92024	3.34060	3.11440	3.46259	3.89736	4.2626	3.59756	3.9123	3.48358	3.11789
	0.75	2.76874	3.10522	2.91325	3.21079	3.63754	4.63109	3.91735	4.28376	3.78868	3.30685
	1.00	2.69839	2.96942	2.80758	3.06026	3.46432	4.84068	4.15719	4.53309	4.02569	3.46432
	0.00	5.36692	5.36692	5.36692	5.36692	5.36692	2.68346	2.68346	2.68346	2.68346	2.68346
Elliptical-paraboloid	0.25	3.42848	3.94626	3.68508	4.06652	4.47243	3.74464	3.27251	3.48182	3.20106	2.98162
	0.50	3.01182	3.45016	3.20941	3.56312	4.02519	4.41157	3.71556	4.05224	3.61172	3.22015
	0.75	2.85638	3.20706	3.00271	3.30339	3.75684	4.79202	4.04583	4.43788	3.93173	3.41531
	1.00	2.78448	3.06681	2.89449	3.14859	3.57794	5.00732	4.29353	4.69569	4.17993	3.57794

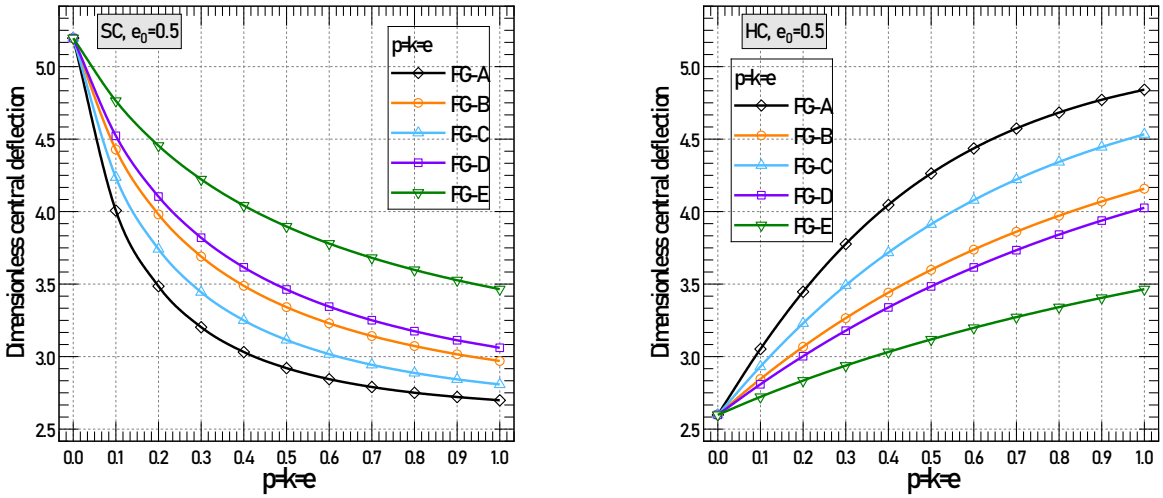

Fig. 5 Effect of power-law parameters "p, k, e" on dimensionless central deflection "$\overline{w}$" for various porous spherical shell (SSSS, $a = b = 10h$)

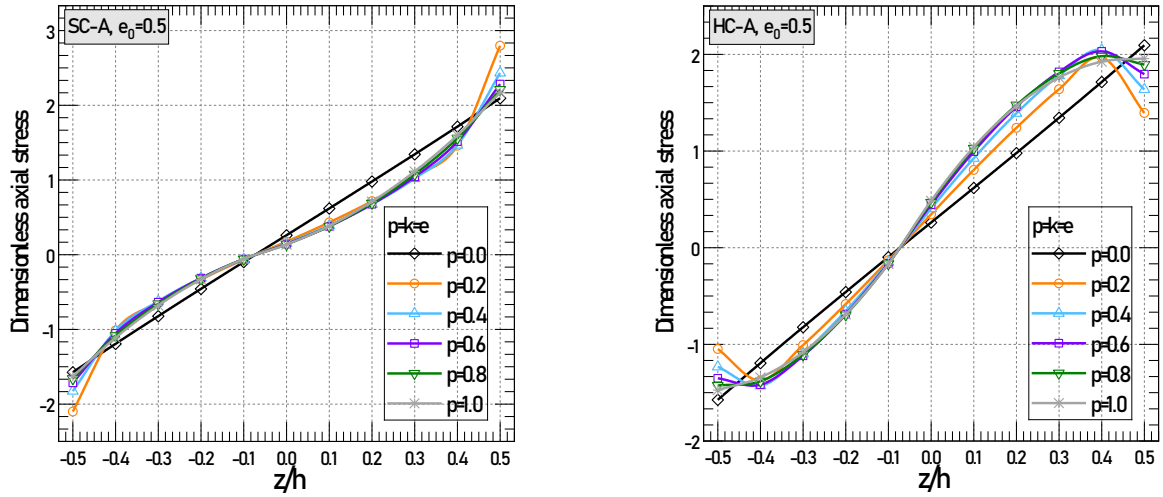

Fig. 6 Effect of power-law parameters "p, k, e" on dimensionless axial stress σ¯_xx of porous spherical shell (SSSS, a=b=10h).

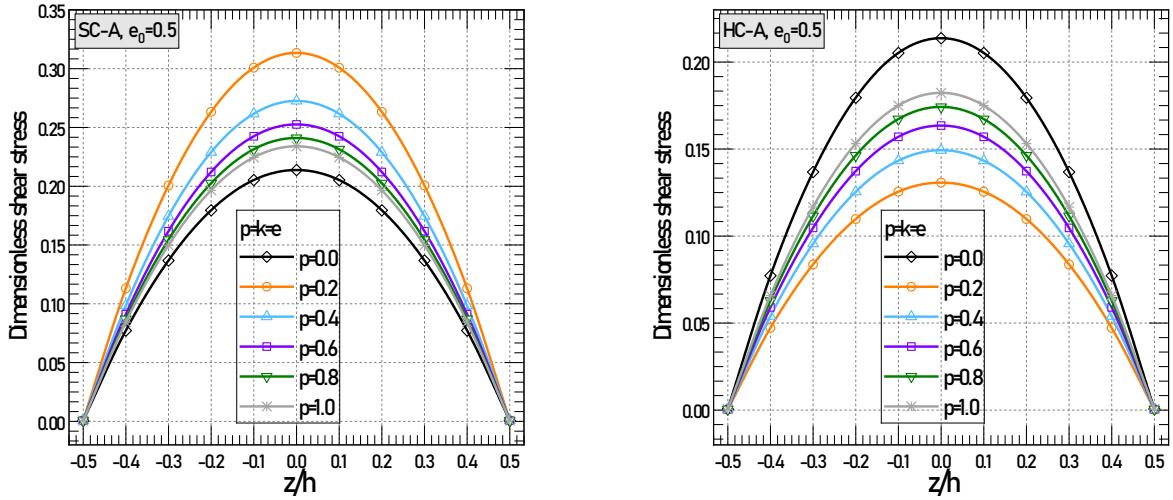

Fig. 7 Effect of power-law parameters "p, k, e" on dimensionless shear stress τ¯_xz of porous spherical shell (SSSS, a=b=10h)

Table 4 Effect of power-law coefficient on dimensionless axial stresses of various patterns of porous shells (e_0=0.5SSSS, a=b=10h)

Shell(*)	p=k=e	SC-A	SC-B	SC-C	SC-D	SC-E	HC-A	HC-B	HC-C	HC-D	HC-E
plate	0.00	2.04636	2.04636	2.04636	2.04636	2.04636	2.04636	2.04636	2.04636	2.04636	2.04636
	0.25	2.59191	1.50468	2.77708	3.0495	1.7053	1.44029	2.49556	1.34101	1.23464	2.27373
	0.50	2.27899	1.31552	2.41648	2.65723	1.53477	1.69969	2.83342	1.56703	1.40283	2.45563
	0.75	2.16483	1.22282	2.26322	2.45932	1.43245	1.84474	3.08528	1.71793	1.53357	2.60446
Cylindrical	1.00	2.11319	1.16935	2.18466	2.34377	1.36424	1.92482	3.27417	1.81707	1.63435	2.72848
	0.00	2.12959	2.12959	2.12959	2.12959	2.12959	2.12959	2.12959	2.12959	2.12959	2.12959
	0.25	2.70223	1.56587	2.89709	3.18426	1.77466	1.49593	2.59706	1.39238	1.28149	2.36621
	0.50	2.37552	1.36902	2.52128	2.77734	1.59719	1.76469	2.94866	1.62552	1.45362	2.55551
Spherical	0.75	2.25577	1.27256	2.36086	2.57115	1.49071	1.91568	3.21077	1.78165	1.58745	2.71039
	1.00	2.20134	1.21691	2.27827	2.45033	1.41973	1.99953	3.40734	1.88466	1.69076	2.83945
	0.00	2.09351	2.09351	2.09351	2.09351	2.09351	2.09351	2.09351	2.09351	2.09351	2.09351
	0.25	2.66794	1.53934	2.86455	3.15537	1.74459	1.46362	2.55306	1.36125	1.25181	2.32612
Hyperbolic-paraboloid	0.50	2.34425	1.34583	2.49378	2.75813	1.57013	1.72499	2.8987	1.58553	1.41411	2.51221
	0.75	2.22431	1.251	2.33387	2.55479	1.46545	1.87355	3.15636	1.73688	1.5404	2.66446
	1.00	2.1692	1.19629	2.25074	2.43462	1.39567	1.95721	3.34961	1.8378	1.63826	2.79134
	0.00	2.11744	2.11744	2.11744	2.11744	2.11744	2.11744	2.11744	2.11744	2.11744	2.11744
Elliptical-paraboloid	0.25	2.69397	1.55694	2.89087	3.18169	1.76454	1.48306	2.58225	1.37973	1.26921	2.35272
	0.50	2.36756	1.36121	2.51637	2.77882	1.58808	1.74851	2.93185	1.60848	1.43603	2.54093
	0.75	2.24712	1.2653	2.3555	2.57341	1.48221	1.89872	3.19245	1.76238	1.5658	2.69493
	1.00	2.192	1.20997	2.27217	2.45242	1.41163	1.98286	3.38791	1.8646	1.6662	2.82326

Table 5 Effect of power-law coefficient on dimensionless shear stresses of various patterns of porous shells (e_0=0.5SSSS, a=b=10h)

Shell(*)	p=k=e	SC-A	SC-B	SC-C	SC-D	SC-E	HC-A	HC-B	HC-C	HC-D	HC-E
plate	0.00	0.23850	0.23850	0.23850	0.23850	0.23850	0.23850	0.23850	0.23850	0.23850	0.23850
	0.25	0.33265	0.35073	0.36919	0.21405	0.39750	0.1525	0.14543	0.13991	0.25364	0.13250
	0.50	0.28980	0.30664	0.32489	0.19870	0.35775	0.1764	0.16511	0.15615	0.26651	0.14310
	0.75	0.27057	0.28503	0.30105	0.18776	0.33390	0.193	0.17979	0.16895	0.27764	0.15177
Cylindrical	1.00	0.26020	0.27257	0.28636	0.17949	0.31800	0.20453	0.19080	0.17916	0.28745	0.15900
	0.00	0.23178	0.23178	0.23178	0.23178	0.23178	0.23178	0.23178	0.23178	0.23178	0.23178
	0.25	0.32376	0.34085	0.35951	0.20859	0.38630	0.14795	0.14133	0.1357	0.24594	0.12877
	0.50	0.28201	0.29800	0.31641	0.19377	0.34767	0.17108	0.16046	0.15133	0.25803	0.13907
Spherical	0.75	0.26322	0.27700	0.29314	0.18314	0.32449	0.18722	0.17472	0.16371	0.26857	0.14749
	1.00	0.25308	0.26489	0.27877	0.17507	0.30904	0.19847	0.18542	0.17361	0.27791	0.15452
	0.00	0.21371	0.21371	0.21371	0.21371	0.21371	0.21371	0.21371	0.21371	0.21371	0.21371
	0.25	0.29973	0.31428	0.33329	0.19377	0.35618	0.13581	0.13031	0.12447	0.22541	0.11873
Hyperbolic-paraboloid	0.50	0.26097	0.27477	0.29341	0.18035	0.32057	0.15690	0.14795	0.1385	0.23556	0.12823
	0.75	0.24340	0.25541	0.2717	0.17054	0.29920	0.17179	0.16111	0.14975	0.24458	0.13600
	1.00	0.23387	0.24424	0.25822	0.16301	0.28495	0.18226	0.17097	0.15886	0.25273	0.14247
	0.00	0.22072	0.22072	0.22072	0.22072	0.22072	0.22072	0.22072	0.22072	0.22072	0.22072
Elliptical-paraboloid	0.25	0.30908	0.32459	0.34349	0.19954	0.36787	0.14051	0.13459	0.12881	0.23334	0.12262
	0.50	0.26915	0.28378	0.30237	0.18559	0.33108	0.16239	0.15281	0.14345	0.24423	0.13243
	0.75	0.25110	0.26379	0.28004	0.17546	0.30901	0.17776	0.16639	0.15514	0.25382	0.14046
	1.00	0.24134	0.25225	0.26621	0.16772	0.29429	0.18853	0.17658	0.16455	0.26242	0.14715

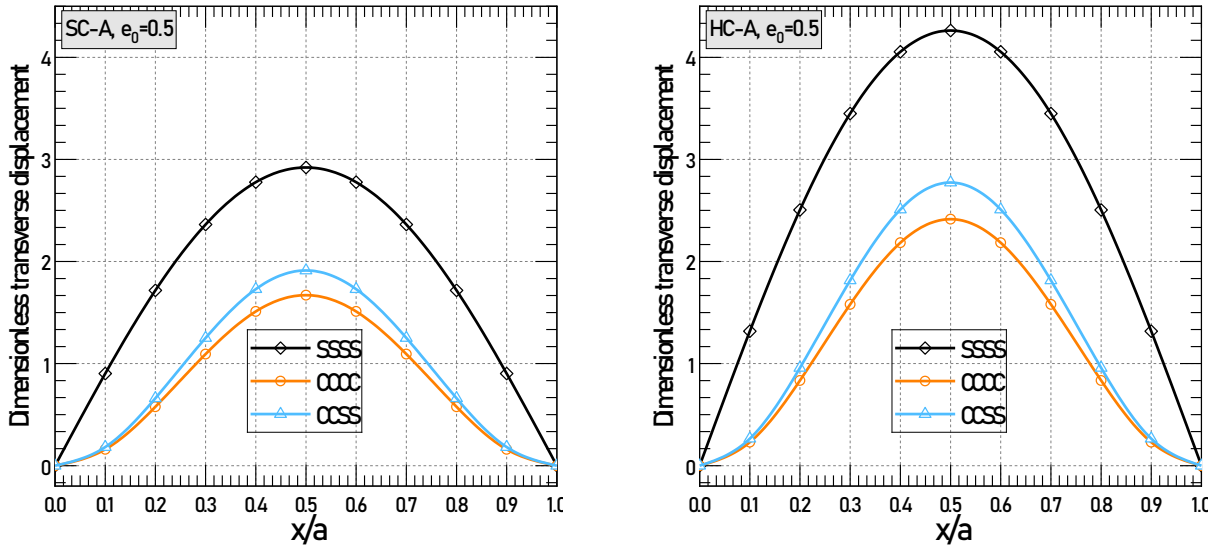

Fig. 8 Dimensionless transverse displacement for various boundary conditions (p=k=e=0. a=b=10h)

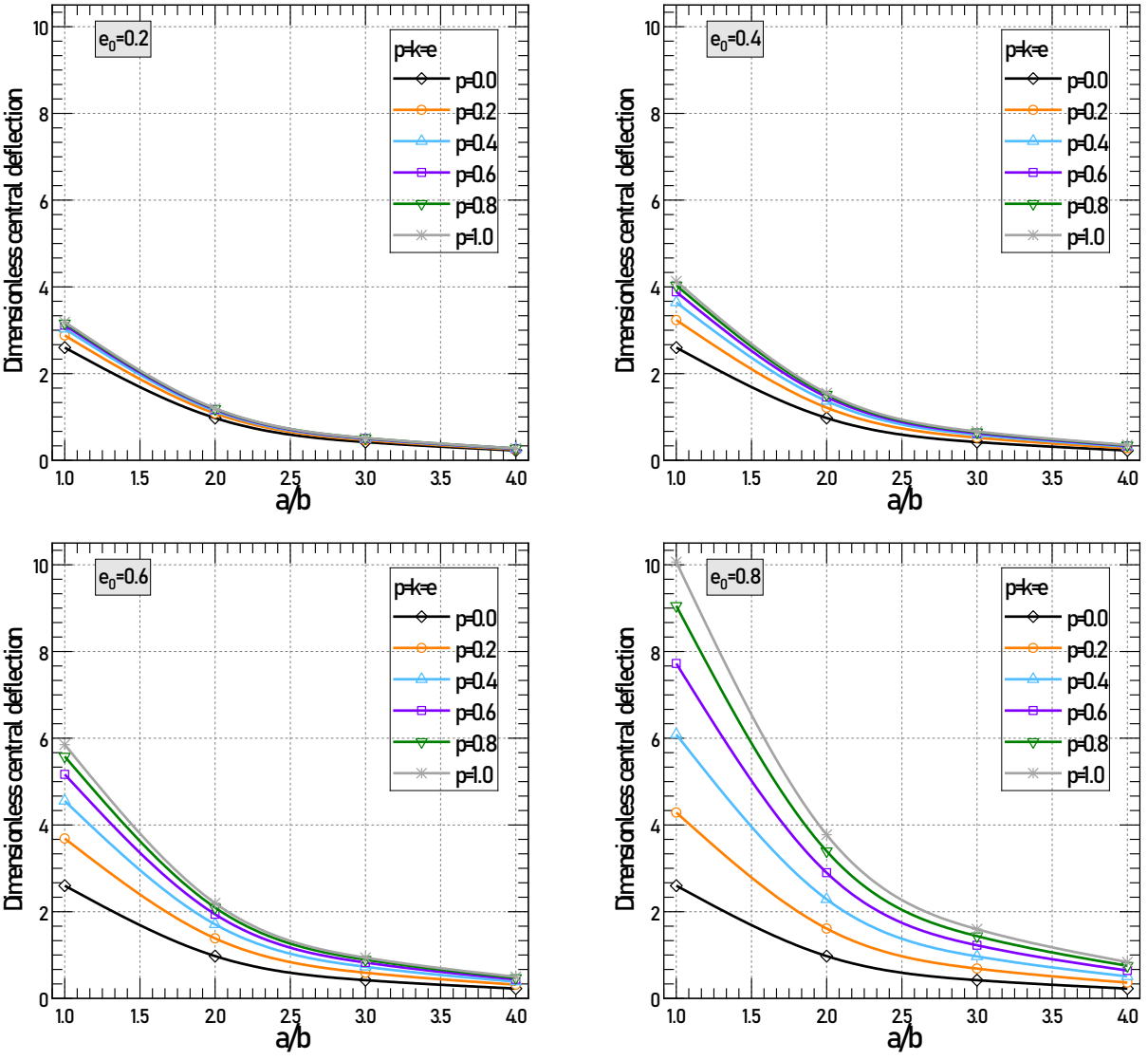

Fig. 9 Effect of aspect ratio "a/b" on dimensionless central deflection of SC porous spherical shell (SSSS, a=10h)

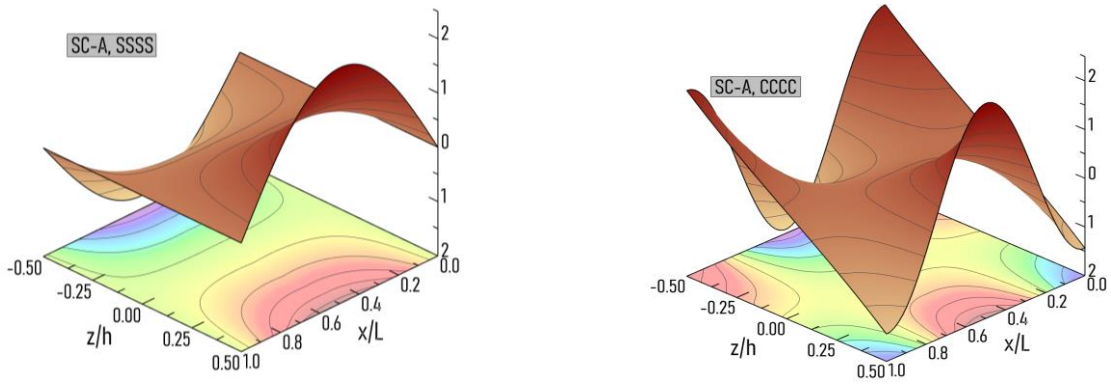

Fig. 10 Dimensionless axial stress σ¯_xx distribution of porous SC spherical shell (p=k=e=e_0=0.5, a=b=10h)

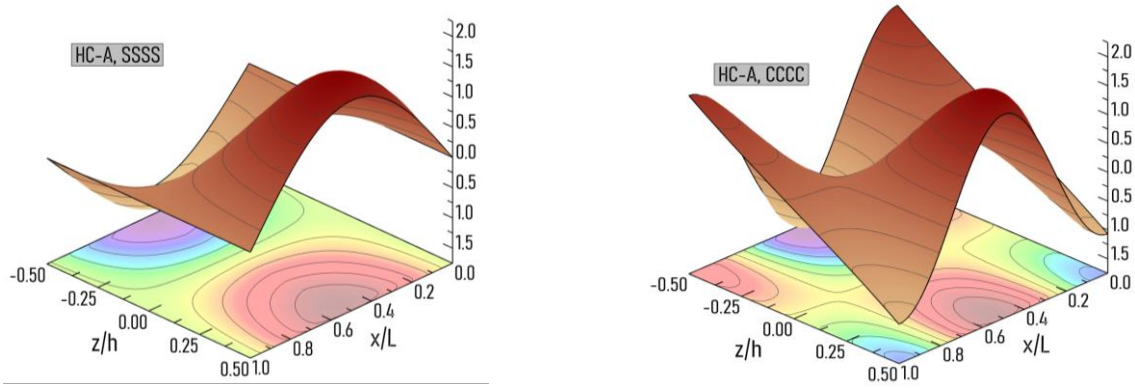

Fig. 11 Dimensionless axial stress σ¯_xx distribution of porous HC spherical shell (p=k=e=e_0=0.5, a=b=10h)

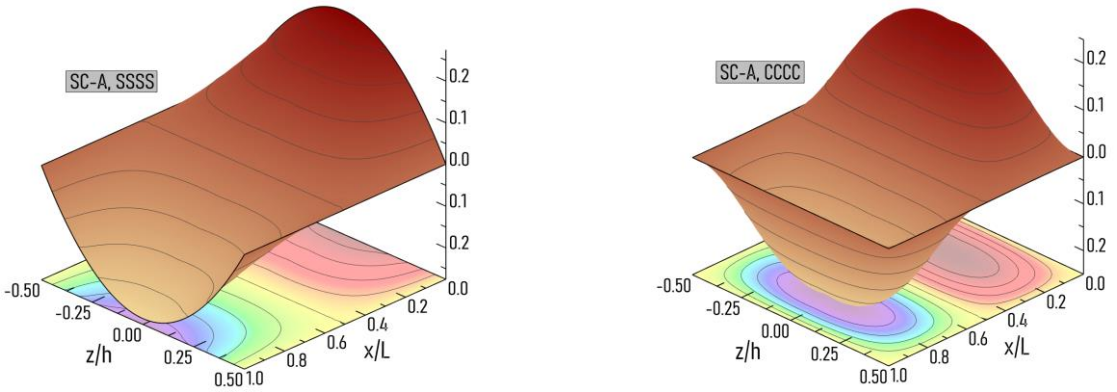

Fig. 12 Dimensionless shear stress "$\bar{\tau}_{xz}$" distribution of porous SC spherical shell ($p = k = e = e_0 = 0.5,\ a = b = 10h$)

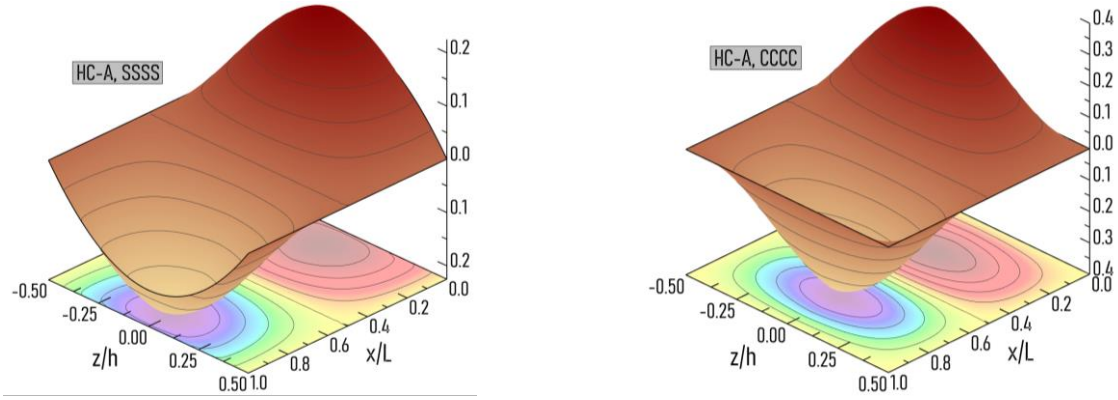

Fig. 13 Dimensionless shear stress "τ¯_xz" distribution of porous HC spherical shell (p=k=e=e_0=0.5, a=b=10h).

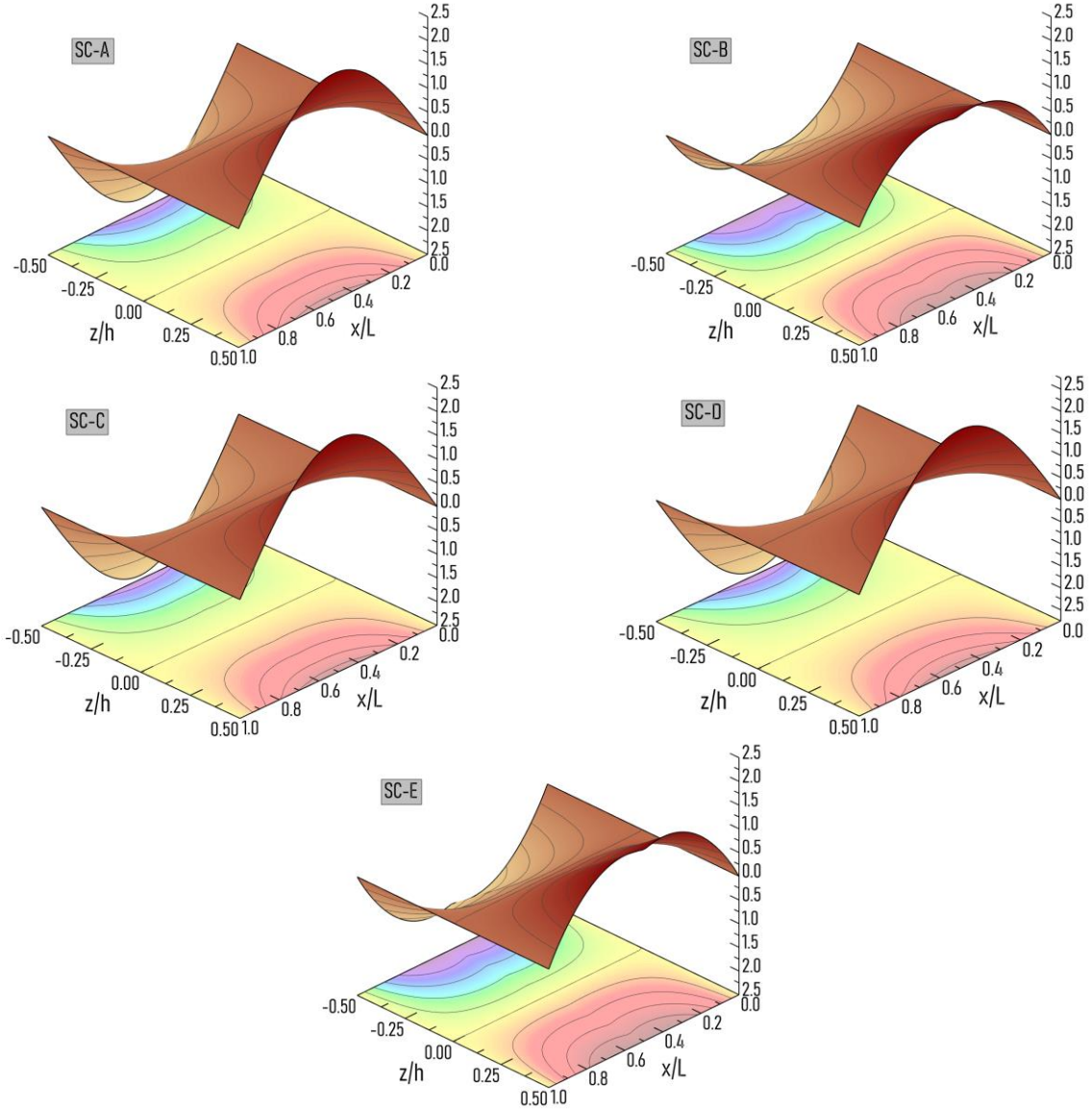

Fig. 14 Dimensionless axial stress distribution of SC porous Elliptical-paraboloid shells (SSSS, p=k=e=e_0=0.5, a=b=10h)

Fig. 7, highlighting the effect of power-law parameters on FG-A porous spherical shells. For SC-A shells, increasing the power-law parameters results in a rise in dimensionless shear stress values. Conversely, HC-A shells exhibit the opposite behavior, with dimensionless shear stress decreasing as the power-law parameters increase.

The dimensionless transverse displacement of FG porous shells is depicted in Figure 8 for both simply supported and clamped boundary conditions. The simply supported shell, being softer and more flexible, exhibits significantly higher displacement compared to the clamped shells.

Fig. 9 presents the dimensionless central deflection of SC porous spherical shells as a function of the aspect ratio, influenced by the porosity coefficient e_0 and the power-law parameters p, k, and e. It is evident that an increase in any of the porosity parameters—p, k, e, or e_0—reduces the overall stiffness of the shell. As a result, the central deflection increases, highlighting the significant role of these parameters in governing the structural flexibility and deformation behavior of porous spherical shells.

Figs. 10 and 11 illustrate the distribution of dimensionless axial stress for various spherical shell boundary conditions, with $p=k=e=e_0=0.5$. The results reveal that tensile stresses dominate the top surface of the shell, while compressive stresses are concentrated at the bottom surface. Notably, the stress values diminish to zero at the edges ($x=0$, L). On the other hand, Figures 12and 13 depict the distribution of shear stress for different SC (soft core) and HC (hard core) porous spherical shell patterns. It is observed that the maximum shear stress values for simply supported shells are concentrated at the mid-plane of the shells.

Figs. 14 and 15 provide a more detailed analysis of the axial stress distributions for various functionally graded (FG) porous shell patterns and schemes.

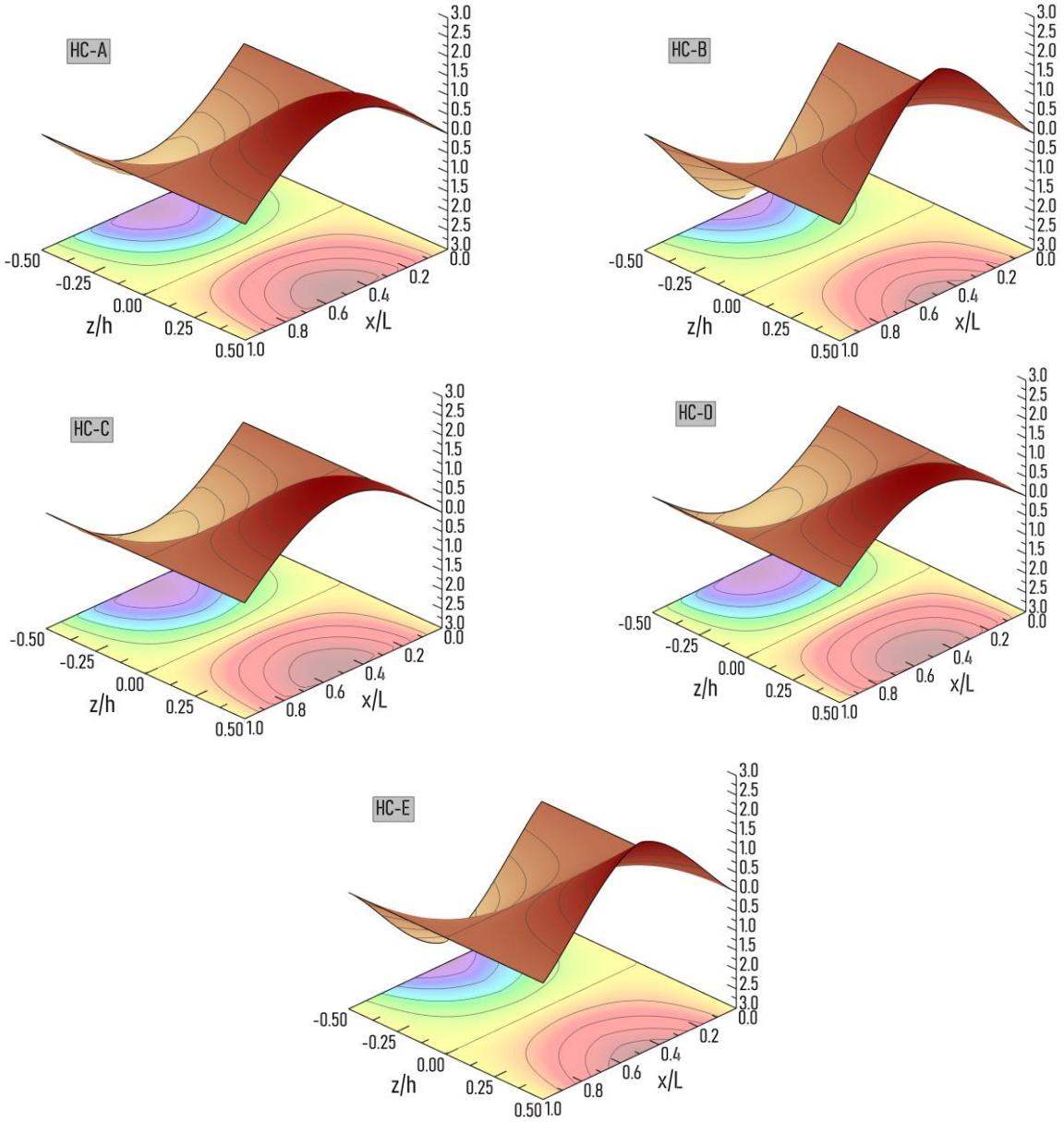

Fig. 15 Dimensionless axial stress distribution of HC porous Elliptical-paraboloid shells (SSSS, p=k=e=e_0=0.5, a=b=10h)

7. Conclusions

This study provides a comprehensive examination of the deflection and stresses in a functionally graded porous shell. The proposed analytical approach is formulated using the modified reduced higher-order theory. The equilibrium equations are derived through the virtual work principle and solved using the Galerkin method. The main findings, obtained from numerical analysis, are summarized as follows:

• For SC shells, increasing power-law parameters *p*, *k*, and *e* reduces central deflection, whereas for HC shells, this trend does not hold.

• Among SC shells, FG-E exhibits the highest rigidity, while for HC shells, HC-A is the most rigid.

• Axial stress distribution depends on porosity coefficient and power-law indices, with maximum stress occurring at the top section of SC shells, regardless of porosity distribution.

• Dimensionless shear stress increases with power-law parameters in SC-A shells, whereas HC-A shells exhibit decreasing shear stress as power-law parameters increase.

• Simply supported shells, being more flexible, experience greater transverse displacement than clamped shells.

• Increasing any of the porosity parameters (*p*, *k*, *e*, e_0) reduces shell stiffness, leading to higher central deflection.

• Axial stress distributions show that tensile stresses dominate the top surface, while compressive stresses concentrate at the bottom surface, with stress values diminishing to zero at the edges.

• Maximum shear stress in simply supported shells is located at the mid-plane of the shells.

References

Abdelhaffez, G.S., Daikh, A.A., Saleem, H.A. and Eltaher, M.A. (2023), "Buckling of coated functionally graded spherical nanoshells resting on an orthotropic elastic medium", *Mathematics*, **11**(2), 409. https://doi.org/10.3390/math11020409

Abouelregal, A.E., Mohammed, W.W. and Mohammad-Sedighi, H. (2021), "Vibration analysis of functionally graded microbeam under initial stress via a generalized thermoelastic model with dual-phase lags", *Arch. Appl. Mech.*, **91**, 2127–2142. https://doi.org/10.1007/s00419-020-01873-2

Belarbi, M.O., Houari, M.S.A., Daikh, A.A., Garg, A., Merzouki, T., Chalak, H.D. and Hirane, H. (2021), "Nonlocal finite element model for the bending and buckling analysis of functionally graded nanobeams using a novel shear deformation theory", *Compos. Struct.*, **264**, 113712. https://doi.org/10.1016/j.compstruct.2021.113712

Chau-Dinh, T. (2023), "Analysis of shell structures using an improved 3-node triangular flat shell element with a bubble function and cell-based strain smoothing", *Thin Wall. Struct.*, **182**, 110222. https://doi.org/10.1016/j.tws.2022.110222

Daikh, A.A., Hamdi, A., Ahmed, H.M., Abdelwahed, M.S., Abdelrahman, A.A. and Eltaher, M.A. (2023), "Buckling and bending of coated functionally graded graphene-reinforced composite plates and shells", *Adv. Nano Res.*, **15**(2), 113-128. https://doi.org/10.12989/anr.2023.15.2.113

Dang, V.H., Sedighi, H.M., Chan, D.Q., Civalek, O. and Abouelregal, A.E. (2021), "Nonlinear vibration and stability of FG nanotubes conveying fluid via nonlocal strain gradient theory", *Struct. Eng. Mech.*, **78**(1), 103-116. https://doi.org/10.12989/sem.2021.78.1.103

Do, V.D., Le Grognec, P. and Rohart, P. (2023), "Closed-form solutions for the elastic–plastic buckling design of shell structures under external pressure", *Eur. J. Mech. A Solids*, **98**, 104861. https://doi.org/10.1016/j.euromechsol.2022.104861

Eroğlu, M., Koç, M.A. and Esen, İ. (2025a), "Thermomechanical free vibration buckling of FG graphene-reinforced doubly-curved sandwich shells", *Adv. Eng. Softw.*, **202**, 103875. https://doi.org/10.1016/j.advengsoft.2025.103875

Eroğlu, M., Koç, M.A. and Esen, İ. (2025b), "3D wave propagation in thermo-mechanical doubly-curved sandwich shells with FG foam core and hybrid faces", *Mech. Based Des. Struct.*, 1-33. https://doi.org/10.1080/15397734.2025.2480393

Esen, I., Garip, Z.S. and Eren, E. (2023), "The effects of the foam and FGM distributions on thermomechanical buckling response of sandwich plates", *Acta Mechanica*, ***235***(2), 1319-1343. https://doi.org/10.1007/s00707-023-03808-8

Garg, A., Belarbi, M.O., Chalak, H.D. and Chakrabarti, A. (2021), "A review of the analysis of sandwich FGM structures", *Compos. Struct.*, **258**, 113427. https://doi.org/10.1016/j.compstruct.2020.113427

Garg, A., Belarbi, M.O., Li, L. and Tounsi, A. (2022), "Bending analysis of power-law sandwich FGM beams under thermal conditions", *Adv. Aircr. Spacecr. Sci.*, **9**(3), 243-261. https://doi.org/10.12989/aas.2022.9.3.243

Garg, A., Belarbi, M.O., Li, L., Chalak, H.D. and Tounsi, A. (2023), "Comparative study on the bending of exponential and sigmoidal sandwich beams under thermal conditions", *Struct. Eng. Mech.*, **85**(2), 217-231. https://doi.org/10.12989/sem.2023.85.2.217

Garg, A., Belarbi, M.O., Tounsi, A., Li, L., Singh, A. and Mukhopadhyay, T. (2022), "Predicting elemental stiffness matrix of FG nanoplates using Gaussian Process Regression based surrogate model in framework of layerwise model", *Eng. Anal. Bound. Elem.*, **143**, 779-795. https://doi.org/10.1016/j.enganabound.2022.08.001

Garg, A., Chalak, H.D., Zenkour, A.M., Belarbi, M.O. and Houari, M.S.A. (2022), "A review of available theories and methodologies for the analysis of nano isotropic, nano functionally graded, and CNT reinforced nanocomposite structures", *Arch. Comput. Meth. Eng.*, **29**, 2237-2270. https://doi.org/10.1007/s11831-021-09652-0

Garg, A., Gupta, S., Chalak, H.D., Belarbi, M.O., Tounsi, A., Li, L. and Zenkour, A.M. (2023), "Free vibration analysis of power-law and sigmoidal sandwich FG plates using refined zigzag theory", *Adv. Mater. Res.*, **12**(1), 43-65. https://doi.org/10.12989/amr.2023.12.1.043

Garg, A., Mukhopadhyay, T., Chalak, H.D., Belarbi, M.O., Li, L. and Sahoo, R. (2022), "Multiscale bending and free vibration analyses of functionally graded graphene platelet/fiber composite beams", *Steel Compos. Struct.*, **44**(5), 707-720. https://doi.org/10.12989/scs.2022.44.5.707

Ghalambaz, M., Aljaghtham, M., Chamkha, A.J., Fteiti, M. and Abdullah, A. (2023), "Latent heat thermal energy storage in a shell-tube: A wavy partial layer of metal foam over tubes", *J. Energy Stor.*, **59**, 106493. https://doi.org/10.1016/j.est.2022.106493

Ghandourah, E.E., Daikh, A.A., Khatir, S., Alhawsawi, A.M., Banoqitah, E.M. and Eltaher, M.A. (2023), "A dynamic analysis of porous coated functionally graded nanoshells resting on a viscoelastic medium", *Mathematics*, **11**(10), 2407. https://doi.org/10.3390/math11102407

Hadji, L., Plevris, V. and Papazafeiropoulos, G. (2024), "Investigation of the static bending response of FGM sandwich plates", *J. Appl. Comput. Mech.*, **10**(1), 26-37. https://doi.org/10.22055/jacm.2023.44278.4194

Hieu, D.V., Chan, D.Q. and Sedighi, H.M. (2021), "Nonlinear bending, buckling and vibration of functionally graded nonlocal strain gradient nanobeams resting on an elastic foundation", *J. Mech. Mater. Struct.*, **16**(3), 327-346. https://doi.org/10.2140/jomms.2021.16.327

Hutchinson, J.W. and He, M.Y. (2000), "Buckling of cylindrical sandwich shells with metal foam cores", *Int. J. Solids Struct.*, **37**(46-47), 6777-6794. https://doi.org/10.1016/S0020-7683(99)00314-5

Jena, S.K., Chakraverty, S., Mahesh, V., Harursampath, D. and Sedighi, H.M. (2022), "Free vibration of functionally graded beam embedded in Winkler-Pasternak elastic foundation with geometrical uncertainties using symmetric Gaussian fuzzy number", *Eur. Phys. J. Plus*, **137**(3), 399. https://doi.org/10.1140/epjp/s13360-022-02607-9

Keleshteri, M.M. and Jelovica, J.J.E.S. (2022), "Analytical solution for vibration and buckling of cylindrical sandwich panels with improved FG metal foam core", *Eng. Struct.*, **266**, 114580. https://doi.org/10.1016/j.engstruct.2022.114580

Khaniki, H.B. and Ghayesh, M.H. (2023), "Highly nonlinear hyperelastic shells: Statics and dynamics", *Int. J. Eng. Sci.*, **183**, 103794. https://doi.org/10.1016/j.ijengsci.2022.103794

Ladmek, M., Belkacem, A., Daikh, A.A., Bessaim, A., Garg, A., Houari, M.S.A., Belarbi, M.O. and Ouldyerou, A. (2023), "Free vibration of functionally graded carbon nanotubes reinforced composite nanobeams", *Adv. Mater. Res.*, **12**(2), 161-177. https://doi.org/10.12989/amr.2023.12.2.161

Medjdoubi, B.A., Houari, M.S.A., Sadoun, M., Bessaim, A., Daikh, A.A., Belarbi, M.O., Khechai, A., Garg, A. and Ghazwani, M.H. (2023), "On the effect of porosity on the shear correction factors of functionally graded porous beams", *Coupled Syst. Mech.*, **12**(3), 199-220. https://doi.org/10.12989/csm.2023.12.3.199

Melaibari, A., Daikh, A.A., Basha, M., Abdalla, A.W., Othman, R., Almitani, K.H., ... and Eltaher, M.A. (2022b), "Free vibration of FG-CNTRCs nano-plates/shells with temperature-dependent properties", *Mathematics*, **10**, 583. https://doi.org/10.3390/math10040583

Melaibari, A., Daikh, A.A., Basha, M., Wagih, A., Othman, R., Almitani, K.H., ... and Eltaher, M.A. (2022a), "A dynamic analysis of randomly oriented functionally graded carbon nanotubes/fiber-reinforced composite laminated shells with different geometries", *Mathematics*, **10**(3), 408. https://doi.org/10.3390/math10030408

Punera, D. and Kant, T. (2019), "A critical review of stress and vibration analyses of functionally graded shell structures", *Compos. Struct.*, **210**, 787-809. https://doi.org/10.1016/j.compstruct.2018.11.084

Radwańska, M., Stankiewicz, A., Wosatko, A. and Pamin, J. (2017), *Plate and Shell Structures: Selected Analytical and Finite Element Solutions*, John Wiley & Sons.

Rizov, V. (2024), "The effect of delamination between layers in U-shaped members made of functionally graded multilayered viscoelastic materials", *J. Appl. Comput. Mech.*, **10**(4), 830-841. https://doi.org/10.22055/jacm.2024.46014.4449

Sedighi, H.M. and Malikan, M. (2020), "Stress-driven nonlocal elasticity for nonlinear vibration characteristics of carbon/boron-nitride hetero-nanotube subject to magneto-thermal environment", *Physica Scripta*, **95**(5), 055218. https://doi.org/10.1088/1402-4896/ab7a38

Sedighi, H.M., Ouakad, H.M., Dimitri, R. and Tornabene, F. (2020), "Stress-driven nonlocal elasticity for the instability analysis of fluid-conveying C-BN hybrid-nanotube in a magneto-thermal environment", *Physica Scripta*, **95**(6), 065204. https://doi.org/10.1088/1402-4896/ab793f

Shariati, A., Jung, D.W., Mohammad-Sedighi, H., Żur, K.K., Habibi, M. and Safa, M. (2020), "On the vibrations and stability of moving viscoelastic axially functionally graded nanobeams", *Materials*, **13**(7), 1707. https://doi.org/10.3390/ma13071707

Son, L.T., Vinh, P.V., Chinh, N.V. and M. Sedighi, H. (2024), "High-frequency temperature-dependent vibration of nonlocal functionally graded sandwich nanoplates resting on elastic foundations", *Mech. Adv. Mater. Struct.*, 1-22. https://doi.org/10.1080/15376494.2024.2358108

Tharwan, M.Y., Daikh, A.A., Assie, A.E., Alnujaie, A. and Eltaher, M.A. (2023), "A comprehensive study on the static response of agglomerated microstructure-dependent coated functionally graded carbon nanotubes reinforced composite nanoshells resting on a complex elastic foundation", *Mech. Based Des. Struct.*, 1-41. https://doi.org/10.1080/15397734.2023.2286484

Tornabene, F., Viscoti, M. and Dimitri, R. (2023), "Static analysis of anisotropic doubly-curved shells subjected to concentrated loads employing higher-order layer-wise theories", *Comput. Model. Eng. Sci.*, **134**(2), 1393-468.

Yıldız, T. and Esen, I. (2023a), "Effect of foam structure on thermo-mechanical buckling of foam core sandwich nanoplates with layered face plates made of functionally graded material (FGM)", *Acta Mechanica*, **234**(12), 6407-6437. https://doi.org/10.1007/s00707-023-03722-z

Yıldız, T. and Esen, I. (2023b), "The effect of the foam structure on the thermomechanical vibration response of smart sandwich nanoplates", *Mech. Adv. Mater. Struct.*, 1-19. https://doi.org/10.1080/15376494.2023.2287179

Appendix

$$K_{11}=A_{11}\int_0^a\int_0^b \frac{\partial^3 X_m}{\partial x^3}Y_n\frac{\partial X_m}{\partial x}Y_n\,dx\,dy+A_{66}\int_0^a\int_0^b \frac{\partial X_m}{\partial x}\frac{\partial^2 Y_n}{\partial y^2}\frac{\partial X_m}{\partial x}Y_n\,dx\,dy$$

$$K_{12}=(A_{12}+A_{66})\left(\int_0^a\int_0^b \frac{\partial X_m}{\partial x}\frac{\partial^2 Y_n}{\partial y^2}\frac{\partial X_m}{\partial x}Y_n\,dx\,dy\right)$$

$$K_{13}=\left(\frac{A_{11}}{R_x}+\frac{A_{12}}{R_y}\right)\left(\int_0^a\int_0^b \frac{\partial X_m}{\partial x}Y_n\frac{\partial X_m}{\partial x}Y_n\,dx\,dy\right)$$

$$-B_{11}\int_0^a\int_0^b \frac{\partial^3 X_m}{\partial x^3}Y_n\frac{\partial X_m}{\partial x}Y_n\,dx\,dy-(B_{12}+2B_{66})\int_0^a\int_0^b \frac{\partial X_m}{\partial x}\frac{\partial^2 Y_n}{\partial y^2}\frac{\partial X_m}{\partial x}Y_n\,dx\,dy$$

$$K_{14}=-C_{11}\int_0^a\int_0^b \frac{\partial^3 X_m}{\partial x^3}Y_n\frac{\partial X_m}{\partial x}Y_n\,dx\,dy-(C_{12}+2C_{66})\int_0^a\int_0^b \frac{\partial X_m}{\partial x}\frac{\partial^2 Y_n}{\partial y^2}\frac{\partial X_m}{\partial x}Y_n\,dx\,dy$$

$$K_{21}=(A_{12}+A_{66})\left(\int_0^a\int_0^b \frac{\partial^2 X_m}{\partial x^2}\frac{\partial Y_n}{\partial y}X_m\frac{\partial Y_n}{\partial y}dx\,dy\right)$$

$$K_{22}=A_{22}\int_0^a\int_0^b X_m\frac{\partial^3 Y_n}{\partial y^3}X_m\frac{\partial Y_n}{\partial y}dx\,dy+A_{66}\int_0^a\int_0^b \frac{\partial^2 X_m}{\partial x^2}\frac{\partial Y_n}{\partial y}X_m\frac{\partial Y_n}{\partial y}dx\,dy$$

$$K_{23}=\left(\frac{A_{12}}{R_x}+\frac{A_{22}}{R_y}\right)\left(\int_0^a\int_0^b X_m\frac{\partial Y_n}{\partial y}X_m\frac{\partial Y_n}{\partial y}dx\,dy\right)-B_{22}\int_0^a\int_0^b X_m\frac{\partial^3 Y_n}{\partial y^3}X_m\frac{\partial Y_n}{\partial y}dx\,dy$$

$$-(B_{12}+2B_{66})\int_0^a\int_0^b \frac{\partial X_m}{\partial x}\frac{\partial^2 Y_n}{\partial y^2}X_m\frac{\partial Y_n}{\partial y}dx\,dy$$

$$K_{24}=-C_{22}\int_0^a\int_0^b X_m\frac{\partial^3 Y_n}{\partial y^3}X_m\frac{\partial Y_n}{\partial y}dx\,dy-(C_{12}+2C_{66})\int_0^a\int_0^b \frac{\partial^2 X_m}{\partial x^2}\frac{\partial Y_n}{\partial y}X_m\frac{\partial Y_n}{\partial y}dx\,dy$$

$$K_{31}=-\left(\frac{A_{11}}{R_x}+\frac{A_{12}}{R_y}\right)\left(\int_0^a\int_0^b \frac{\partial^2 X_m}{\partial x^2}Y_nX_mY_n\,dx\,dy\right)+B_{11}\int_0^a\int_0^b \frac{\partial^4 X_m}{\partial x^4}Y_nX_mY_n\,dx\,dy$$

$$+(B_{12}+2B_{66})\int_0^a\int_0^b \frac{\partial^2 X_m}{\partial x^2}\frac{\partial^2 Y_n}{\partial y^2}X_mY_n\,dx\,dy$$

$$K_{32}=-\left(\frac{A_{12}}{R_x}+\frac{A_{22}}{R_y}\right)\left(\int_0^a\int_0^b X_m\frac{\partial^2 Y_n}{\partial y^2}X_mY_n\,dx\,dy\right)+B_{22}\int_0^a\int_0^b X_m\frac{\partial^4 Y_n}{\partial y^4}X_mY_n\,dx\,dy$$

$$+(B_{12}+2B_{66})\int_0^a\int_0^b \frac{\partial^2 X_m}{\partial x^2}\frac{\partial^2 Y_n}{\partial y^2}X_mY_n\,dx\,dy$$

$$K_{33}=2\left(\frac{B_{11}}{R_x}+\frac{B_{12}}{R_y}\right)\left(\int_0^a\int_0^b \frac{\partial^2 X_m}{\partial x^2}Y_nX_mY_n\,dx\,dy\right)+2\left(\frac{B_{12}}{R_x}+\frac{B_{22}}{R_y}\right)\left(\int_0^a\int_0^b X_m\frac{\partial^2 Y_n}{\partial y^2}X_mY_n\,dx\,dy\right)$$

$$-\left(\frac{A_{11}}{R_x^2}+2\frac{A_{12}}{R_xR_y}+\frac{A_{22}}{R_y^2}\right)\left(\int_0^a\int_0^b X_mY_nX_mY_n\,dx\,dy\right)-D_{11}\int_0^a\int_0^b \frac{\partial^4 X_m}{\partial x^4}Y_nX_mY_n\,dx\,dy$$

$$-D_{22}\left(\int_0^a\int_0^b X_m\frac{\partial^4 Y_n}{\partial y^4}X_mY_n\,dx\,dy\right)-2(D_{12}+2D_{66})\int_0^a\int_0^b \frac{\partial^2 X_m}{\partial x^2}\frac{\partial^2 Y_n}{\partial y^2}X_mY_n\,dx\,dy$$

$$K_{34}=-\left(\frac{C_{11}}{R_x}+\frac{C_{12}}{R_y}\right)\left(\int_0^a\int_0^b \frac{\partial^2 X_m}{\partial x^2}Y_nX_mY_n\,dx\,dy\right)-\left(\frac{C_{12}}{R_x}+\frac{C_{22}}{R_y}\right)\left(\int_0^a\int_0^b X_m\frac{\partial^2 Y_n}{\partial y^2}X_mY_n\,dx\,dy\right)$$

$$-E_{11}\int_0^a\int_0^b \frac{\partial^4 X_m}{\partial x^4}Y_nX_mY_n\,dx\,dy-E_{22}\left(\int_0^a\int_0^b X_m\frac{\partial^4 Y_n}{\partial y^4}X_mY_n\,dx\,dy\right)$$

$$-2(E_{12}+2E_{66})\int_0^a\int_0^b \frac{\partial^2 X_m}{\partial x^2}\frac{\partial^2 Y_n}{\partial y^2}X_mY_n\,dx\,dy$$

$$K_{41} = C_{11}\int_0^a\int_0^b \frac{\partial^4 X_m}{\partial x^4} Y_n X_m Y_n \, dx\, dy + (C_{12} + 2C_{66})\int_0^a\int_0^b \frac{\partial^2 X_m}{\partial x^2}\frac{\partial^2 Y_n}{\partial y^2} X_m Y_n \, dx\, dy$$

$$K_{42} = C_{22}\int_0^a\int_0^b X_m \frac{\partial^4 Y_n}{\partial y^4} X_m Y_n \, dx\, dy + (C_{12} + 2C_{66})\int_0^a\int_0^b \frac{\partial^2 X_m}{\partial x^2}\frac{\partial^2 Y_n}{\partial y^2} X_m Y_n \, dx\, dy$$

$$K_{43} = -\left(\frac{C_{11}}{R_x} + \frac{C_{12}}{R_y}\right)\left(\int_0^a\int_0^b \frac{\partial X_m}{\partial x} Y_n \frac{\partial X_m}{\partial x} Y_n \, dx\, dy\right) - \left(\frac{C_{12}}{R_x} + \frac{C_{22}}{R_y}\right)\left(\int_0^a\int_0^b X_m \frac{\partial Y_n}{\partial y} X_m \frac{\partial Y_n}{\partial y} dx\, dy\right)$$
$$-E_{11}\int_0^a\int_0^b \frac{\partial^4 X_m}{\partial x^4} Y_n X_m Y_n \, dx\, dy - E_{22}\left(\int_0^a\int_0^b X_m \frac{\partial^4 Y_n}{\partial y^4} X_m Y_n \, dx\, dy\right)$$
$$-2(E_{12} + 2E_{66})\int_0^a\int_0^b \frac{\partial^2 X_m}{\partial x^2}\frac{\partial^2 Y_n}{\partial y^2} X_m Y_n \, dx\, dy$$

$$K_{44} = -F_{11}\int_0^a\int_0^b \frac{\partial^4 X_m}{\partial x^4} Y_n X_m Y_n \, dx\, dy - F_{22}\left(\int_0^a\int_0^b X_m \frac{\partial^4 Y_n}{\partial y^4} X_m Y_n \, dx\, dy\right)$$
$$-2(F_{12} + 2F_{66})\int_0^a\int_0^b \frac{\partial^2 X_m}{\partial x^2}\frac{\partial^2 Y_n}{\partial y^2} X_m Y_n \, dx\, dy + J_{44}\int_0^a\int_0^b X_m \frac{\partial^2 Y_n}{\partial y^2} X_m Y_n \, dx\, dy$$
$$+J_{55}\int_0^a\int_0^b \frac{\partial^2 X_m}{\partial x^2} Y_n X_m Y_n \, dx\, dy$$